A Novel Octagonal-Shaped UWB Patch Antenna for V2X, WIMAX, WLAN and Wi-Fi 6 /Wi-Fi 6E communications

Omar Ourahou[1], Fatima Ez-zaki[1], Saida Ibnyaich[3], Hassan Belahrach[2] and Abdelilah Ghammaz[1]

[1]Laboratory of Electrical systems, Energy efficiency and Telecommunications (LSEEET), Department of Physics, Faculty of Sciences and Techniques Gueliz, Cadi Ayyad University, Marrakech, Morocco
[2]Laboratory of Electrical Engineering Royal School of Aeronautics *Marrakesh, Morocco*
[3]Laboratory of Instrumentation Signals and Physical Systems (I2SP) Department of physics, Faculty of Science Cadi Ayyad University Marrakech, Morocco

Corresponding author: OURAHOU, OMAR (o.ourahou.ced@uca.ac.ma).

ABSTRACT A novel octagonal-shaped ultra-wideband (UWB) microstrip antenna is proposed for vehicle-to-everything (V2X) communications based on Dedicated Short-Range Communications (DSRC/IEEE 802.11p at 5.9 GHz) and for multi-standard wireless systems. The antenna operates from 4.2 to 8.9 GHz, providing a 4.7 GHz impedance bandwidth for $S11| \leq -10$ dB. This wideband response simultaneously covers WiMAX, WLAN IEEE 802.11ac/n (5.2 and 5.8 GHz), Wi-Fi 6, Wi-Fi 6E, and 5G sub-6 GHz applications. The simulated realized gain varies from 2.46 dBi to 5.15 dBi over the operating band. A prototype is fabricated and characterized using a 3656D vector network analyzer. The measured resonances at 4.22, 6.04, and 8.04 GHz closely match the simulated ones at 4.2, 5.84, and 8.01 GHz, with a maximum frequency deviation below 3.5%. The measured reflection minima (−13.30, −20.20, and −14.18 dB) differ by less than 4 dB from the simulated values (−14.23, −19.23, and −17.78 dB), and the measured operating bandwidth (4.2–8.9 GHz) is consistent with the simulated 4.2–8.71 GHz range. These results confirm the suitability of the proposed compact antenna for integrated UWB V2X/DSRC front-ends and emerging 5G/Wi-Fi 6/6E systems.

INDEX TERMS vehicular communications, WLAN, 5G, HFSS, Wi-Fi.

INTRODUCTION

Over the past few years, there has been rapid advancement in Internet of Things (IoT) technology. Within this concept, vehicle networking has emerged as a crucial component. The vehicular communication is coming to offer a driving comfort, to avoid road accidents, to ensure road safety, and to save time[1]. Cellular Vehicle-to-Everything (C-V2X) and Dedicated Short Range Communication (DSRC) stand as the primary technologies widely utilized worldwide [2]. DSRC based on IEEE 802.11p protocol is adopted at 5 GHz in almost countries including the USA (5.850-5.925 GHz), Europe (5.875-5.905 GHz) in 2008, and Japan use (5.770-5.850 GHz). DSRC, operating on the IEEE 802.11p protocol, is implemented at 5 GHz in numerous countries, including the USA (5.85-5.9250 GHz) and Europe (5.8750-5.9050 GHz) since 2008. In Japan, it operates within the (5.770-5.850 GHz) spectrum.

Microstrip patch antennas (MPAs) offer numerous advantages within communication systems due to their compact size, cost-effectiveness, and seamless integration into peripheral devices, rendering them well-suited for such communication applications[3].

Ultra-Wide Band (UWB) technology has sparked substantial interest in cutting-edge wireless communications following the US Federal Communications Commission (FCC) declaration allowing the use of the 3.10–10.60 GHz band for commercial communication applications in ultra-wideband systems. Its attractiveness stems from its cost-effectiveness, simplified design, excellent data precision, notably low spectral power density, limited interference, and exceptionally high data transfer speeds. These enticing attributes position it as a highly promising choice for contemporary wireless communication systems [4]. UWB technology holds significant importance within radar applications [5],[6] as well as in communication systems

[7],[8]. The primary obstacle in UWB antenna design involves attaining a significantly wide bandwidth while maintaining high radiation efficiency and compact dimensions[9]. Additionally, the modern wireless communication systems employ compact electronic devices and components. However, antennas often occupy substantial real estate within these devices. Consequently, the need for miniaturized, compact, and low-profile antennas is critical. Yet, designing such antennas remains an immensely challenging task, continuing to be a prominent area of research in both past and present times [10]. Antenna miniaturization have been discussed in [11]. As previously mentioned, the use of slots can improve the antenna bandwidth. For instance, in [12], the author expanded the antenna bandwidth by integrating a dual-slot into a rectangular patch. Therefore, in [13] a compact antenna with expanded bandwidth is suggested by incorporating slots. The antennas proposed in [14],[15] achieve UWB through the use of slots; however, these antennas possess a larger volume.

On the other hand, numerous antennas have been suggested for V2X communications. For instance, the study outlined in [16]-[17] introduces a unique antenna model tailored specifically for V2V communications, compatible with LTE and the IEEE 802.11 standard.

In [18], a quad-element MIMO antenna for 5.9 GHz V2X communications is reported, offering only 85 MHz of impedance bandwidth. The antenna presented in [19] provides an even narrower bandwidth of 10 MHz. In [20], the author proposes another antenna for V2X communication, where only 5 MHz of bandwidth is achieved. In [21], a compact antenna for V2X at 5.9 GHz is proposed, providing a bandwidth of 180 MHz with overall dimensions of 55 mm × 60 mm × 1 mm. In [22], a fractal MIMO antenna for V2X at 5.91 GHz and X-band operation at 9.67 GHz is introduced, exhibiting bandwidths of 1.49 GHz and 2.77 GHz, respectively.

In this work, we propose a low-cost and compact ultra-wideband (UWB) antenna designed for various V2X and wireless communication applications. The antenna covers the DSRC/IEEE 802.11p band (5.850–5.925 GHz) and Cellular V2X (C-V2X) operation around 5.9 GHz in the 5G sub-6 GHz range. In addition, it accommodates other wireless standards, including the 5G sub-6 GHz n79 band (4.40–5.00 GHz), IEEE 802.11ac/n WLAN (5.20 and 5.80 GHz), the WiMAX band at 5.80 GHz, Wi-Fi 6 based on the IEEE 802.11ax protocol (5.150–7.125 GHz), and Wi-Fi 6E (5.925–7.125 GHz), as well as the emerging 6G bands in the ranges 6.425–7.125 GHz and 7.125–8.4 GHz

II. Antenna design and geometry

In this section, the mathematical modeling and the parametric study of the proposed antenna are discussed. Based on the cavity model, the resonant frequency of the fundamental mode of a circular patch antenna is obtained using (1) [23].

the mathematical modeling and the parameter study will be discussed in this section.

$$F_r = \frac{CX_{np}}{2\pi a_{eff}\sqrt{\epsilon_r}} \quad (1)$$

Where εr denotes the relative permittivity of the substrate, c is the speed of light in free space, and Xnp represents the zeros of the derivative of the Bessel function Bn(x), which have characteristics similar to those of TE modes in circular waveguides. For the fundamental TM11 mode, X11 = 1.841180. The parameter a_{eff} denotes the effective radius of the patch, considering fringing-field effects. As is well known, these fringing fields increase the electrical size of the patch; this effect is commonly modeled by introducing a correction factor. For a circular patch, this correction is expressed in terms of the effective radius a_{eff} instead of the physical radius a, as described in [23]:

$$a_{eff} = \sqrt{a^2\left(1+\frac{2h}{\pi a\epsilon_r}\left(ln\left(\frac{\pi a}{2h}\right)+1.7726\right)\right)} \quad (2)$$

Here, h denotes the thickness of the substrate in cm. For a_{eff} and a within the logarithmic function. This process results in:

$$a = \frac{F}{\sqrt{\left(1+\frac{2h}{\pi F\epsilon_r}\left(ln\left(\frac{\pi F}{2h}\right)+1.7726\right)\right)}} \quad (3)$$

Where:

$$F = \frac{8.791\times 10^9}{F_r\times\sqrt{\epsilon_r}} \quad (4)$$

In order to design the regular octagonal patch, we adopt the area–equivalence approach proposed in [17]. In this method, the noncircular radiator is obtained by equating its area to that of an equivalent circular patch derived from the cavity model. First, the area of the circular patch with effective radius aeff is written as:

$$area_{\ circle} = \pi \times a^2 \quad (5)$$

whereas the area of a regular octagon with side length:

$$area_{octagon} = 2\times\left(1+\sqrt{2}\right)\times d^2 \quad (6)$$

By equating these two areas and solving for d, we obtain by (6):

$$d = 0.8a_{eff} \quad (7)$$

Therefore, the coefficient 0.8 does not correspond to an empirical tuning factor, but directly results from the geometrical relation between the equivalent circular patch and the regular octagon within the area–equivalence approach described in [17].

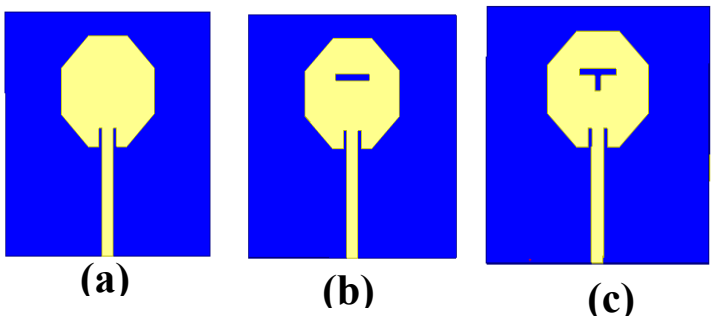

FIGURE 1. Geometry evolution of the proposed antenna: (a) Step 1, (b) Step 2, and (c) Step 3.

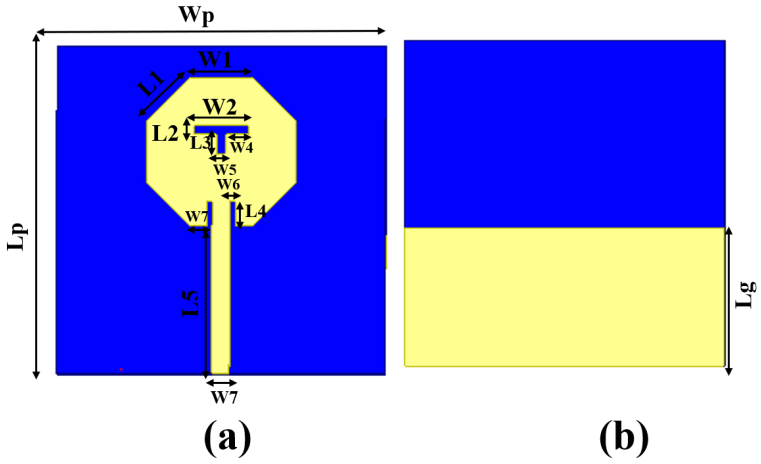

FIGURE 2. Final configuration of the proposed antenna.

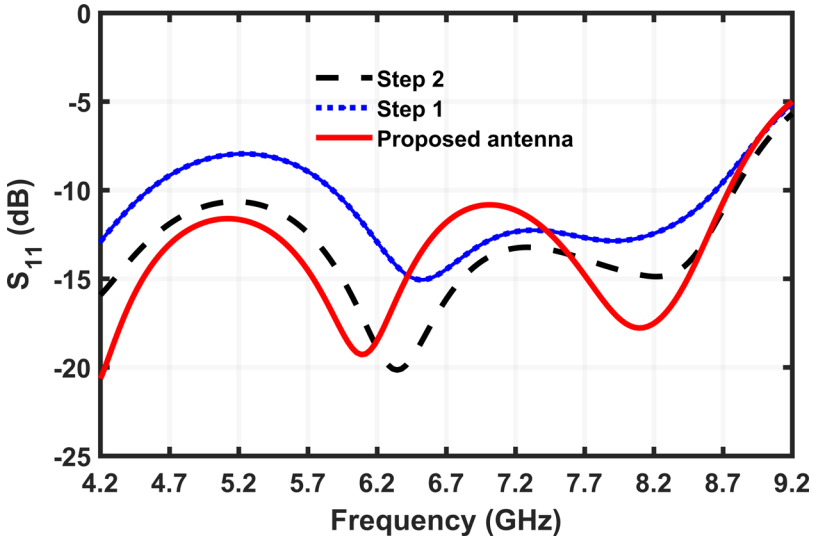

FIGURE 3. Corresponding return-loss characteristics of the proposed antenna for the different design steps.

An FR-4 epoxy substrate with a thickness of 1.6 mm, a relative dielectric permittivity of 4.4, and a loss tangent of 0.0028 is used to design the proposed antenna, which is fed through an SMA connector. The proposed antenna is optimized using HFSS.

The design of the proposed antenna is refined through several iterations, as illustrated in Fig. 1. In the first step, an octagonal patch (Step 1) operates over the 5.6–8.6 GHz band with S11 < –10 dB, but no resonance is obtained at the desired 5.9 GHz frequency. In the second step, a rectangular slot is etched in the radiating patch (Step 2), which improves

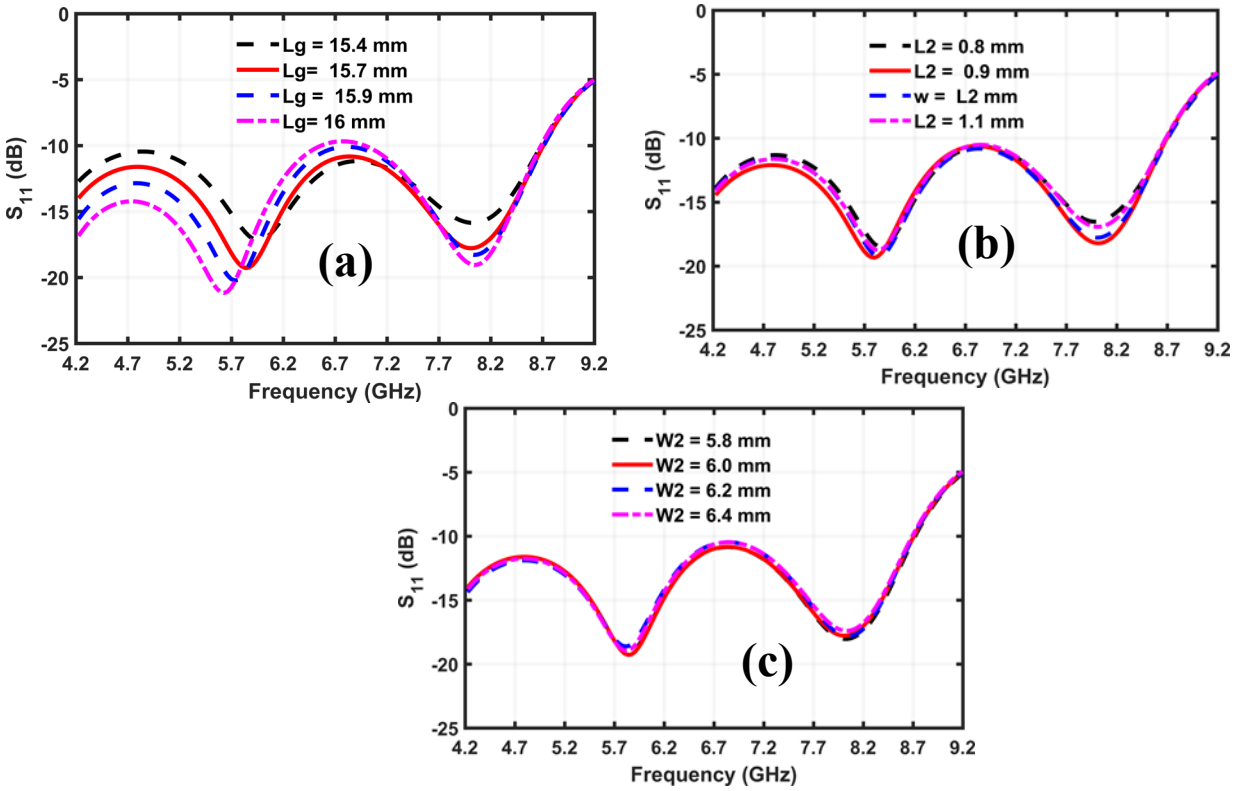

FIGURE 4. Simulated reflection coefficient S11 of the proposed antenna for different values of (a) ground–plane length Lg, (b) slot length L2 , and (c) slot width W2.

impedance matching and slightly broadens the bandwidth. However, the antenna still fails to produce a distinct resonance around 5.9 GHz. In the third step (Step 3), an additional vertical slot is introduced, forming a T-shaped slot. This configuration effectively perturbs the surface current distribution, increases the effective electrical length of the patch, and shifts the resonance toward the target frequency. As a result, a clear resonance appears at 5.9 GHz while maintaining a wide operational bandwidth.

The simulated S11 characteristics of the three configurations are plotted in Fig. 3, confirming the progressive improvement in impedance matching and bandwidth with each design iteration.

Fig. 2 shows the layout of the proposed antenna, including the design parameters of the radiating patch, feed line, and partial ground plane.

Table I illustrates the final values of the dimensions of the suggested antenna.

TABLE I. Dimensions of the suggested antenna.

Dimension	Value(mm)	Dimension	Value(mm)
Wp	36	L1	6.96
Lp	36	W2	6
W1	6.96	L2	1
L3	2.2	W4	2.5
W5	1	W7	1.88
W6	0.6	W8	2
L4	2.8	L5	19.39
Lg	15.7	h	1.6

Fig. 4(a) shows the influence of the partial ground-plane length Lg on the S11 response. It is observed that varying Lg causes a noticeable shift in the resonance frequencies and changes the impedance bandwidth. This occurs because the partial ground plane forms, together with the feed line, a strong capacitive coupling region. Increasing Lg increases the capacitive loading seen by the patch, which results in poorer impedance matching and a downward shift of the resonances. Conversely, reducing Lg reduces this capacitive effect but may degrade bandwidth. An optimal value of Lg = 15.7 mm provides a good compromise, ensuring proper impedance matching and stable resonance around 5.9 GHz. Table II summarizes the obtained performance at each step of the antenna evolution.

TABLE II. Comparison of operating band, resonant frequencies, and S11 levels for the different design steps.

	Step 1	Step 2	Proposed antenna
Operating band (GHz)	5.6–8.6	4.2–8.75	4.2–8.9
Resonant frequency (GHz)	6.29	6.20; 6.11; 8.14	4.20; 5.84; 8.01
S11 (dB)	-15	-12.69; -20.15; -14.87	-14.23; -19.23; -17.78

Fig. 4(b) illustrates the effect of the slot length L2 on the reflection coefficient. As L2 increases, the resonance frequencies shift and the return-loss levels improve. The

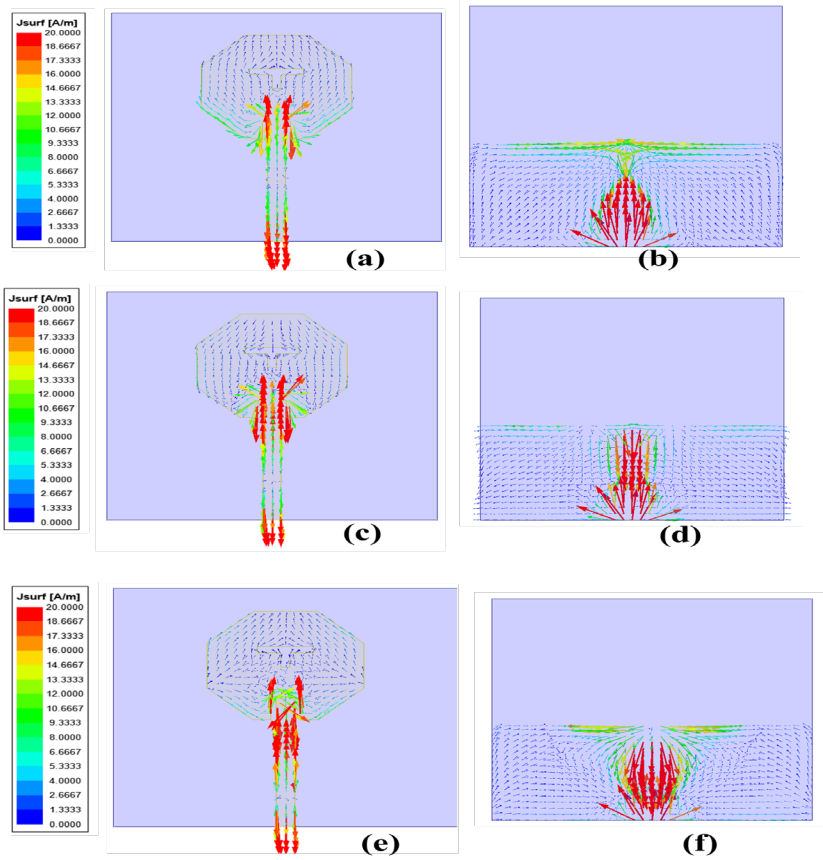

FIGURE 5. Vector current surface at 4.2 GHz: (a) top and (b) button view Vector current surface at 5.84 GHz: (c) top and (d) button view. Vector current surface at 8.01 GHz: (e) top and (f) button view

reason is that the slot introduces an additional current path, effectively increasing the electrical length of the radiator. A longer slot forces the surface current to travel further before reaching the open edge, which lowers the resonant frequency. When L2 = 1 mm, the effective path length becomes properly tuned, leading to optimum impedance matching around 5.9.

Fig. 4(c) presents the variation in S11 for different values of W2. Increasing W2 modifies the coupling between the slot and the surrounding patch region. A wider slot increases the perturbation of the current distribution and enhances the capacitive effect around the slot edges, which improves impedance matching but may slightly influence bandwidth. The optimum case is obtained at W2 = 6 mm, where the balance between coupling and radiation efficiency is achieved.

The surface current distributions at the resonant frequencies provide further insight into the effect of the design parameters. At 4.2 GHz, the current is mainly concentrated along the feed line and the lower part of the radiating patch, indicating that the effective electrical length is dominated by the path between the feed and the ground-plane edge. When the frequency increases to 5.84 GHz, a significant portion of the current is concentrated around the T-shaped slot. The slot forces the current to follow a longer path around its edges, effectively increasing the resonant electrical length and improving impedance matching around 5.9 GHz. At 8.01 GHz, the current becomes more localized near the upper edges of the patch, corresponding to a higher-order mode with shorter current loops.

These observations explain the results of the parametric study. Changing the ground-plane length Lg modifies the coupling between the feed and ground, altering the lower-band resonance. Adjusting the slot length L2 changes the current path around the slot, thereby tuning the 5.9 GHz resonance. Finally, varying the slot width W2 affects the coupling strength and capacitive loading in the slot region, influencing both bandwidth and matching. The optimized geometry ensures that the dominant currents are concentrated along the T-shaped slot and feed region, leading to stable resonance around 5.9 GHz while maintaining UWB performance.

III. Results and discussion

After completing the optimization of the proposed antenna using HFSS software, the design is physically fabricated to validate the simulation outcomes. The performance of the

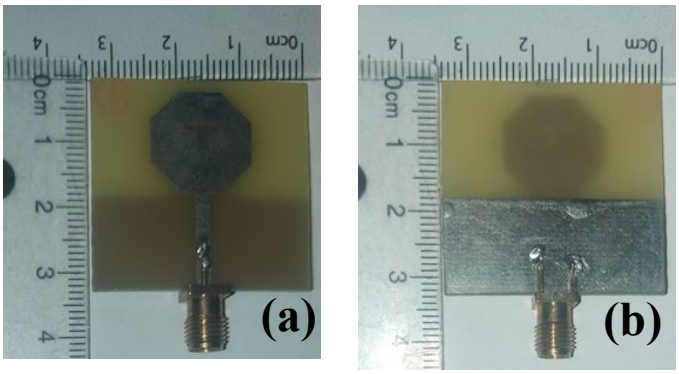

FIGURE 6. Fabricated prototype of the proposed antenna.

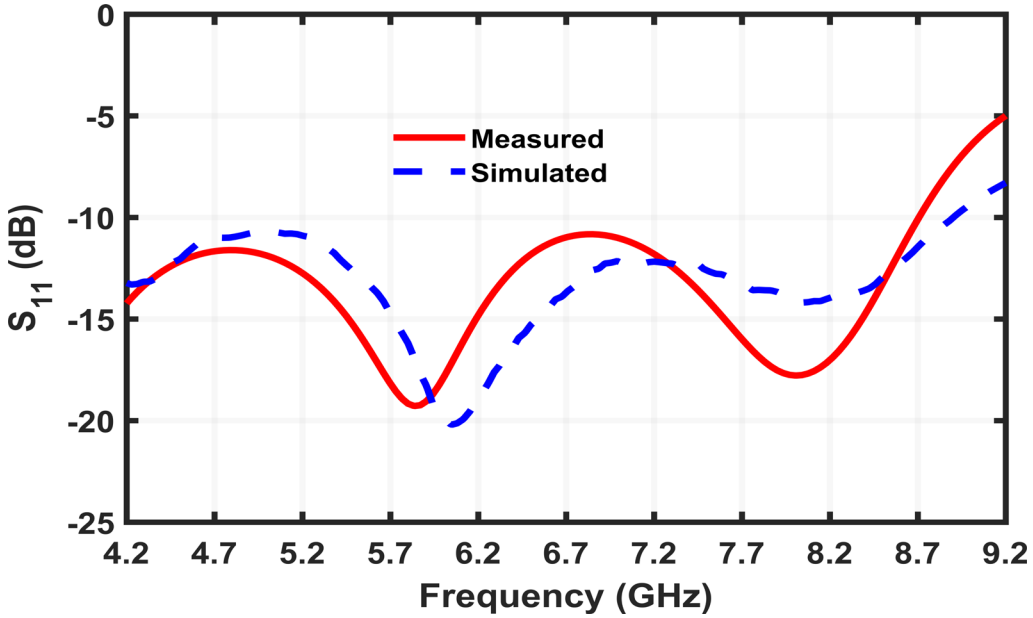

FIGURE 7. Simulated and measured return loss coefficient of the proposed antenna

fabricated antenna is then evaluated through experimental measurements using a 3656D vector network analyzer, ensuring that the observed results align with the predicted behavior.

TABLE III. Comparative Analysis of Simulation and Measured Results in Terms of S11

	Resonant frequency (GHz)	S11 (dB)	Operating bandwidth (GHz)
Measured results	4.22; 6.04; 8.04	-13.30; -20.20; -14.18	4.2-8.9
Simulated results	4.2; 5.84; 8.01	-14.23; -19.23; -17.78	4.2-8.71

Fig. 7 presents a comparison between the simulated and measured S11 characteristics of the proposed antenna. The results show that the antenna achieves a –10 dB bandwidth of 4.51 GHz in simulations (HFSS), while the measured bandwidth extends to 4.7 GHz. Overall, the measured and simulated responses exhibit a strong level of agreement, confirming the reliability of the design approach. Minor discrepancies between the two results can be attributed to fabrication tolerances, such as slight variations in substrate thickness or etching accuracy, as well as the influence of the SMA connector, which introduces parasitic effects not fully captured in the simulation model. In addition, measurement setup uncertainties, including cable losses and calibration errors of the vector network analyzer, may also contribute to the observed differences. For clarity, a summary of the S11 values from both simulation and measurement is provided in Table III, highlighting the consistency between numerical predictions and experimental validation. These outcomes demonstrate that the antenna effectively supports a wide range of

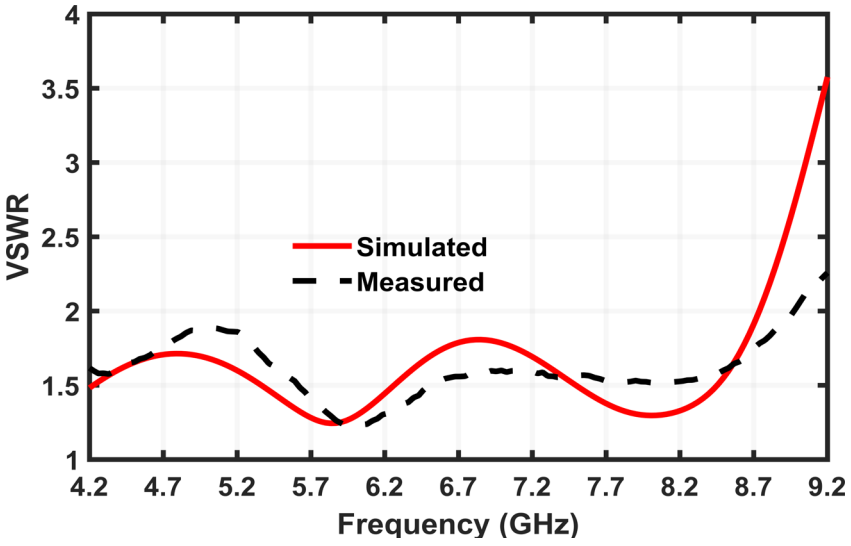

FIGURE 8. Simulated and measured VSWR of the suggested antenna

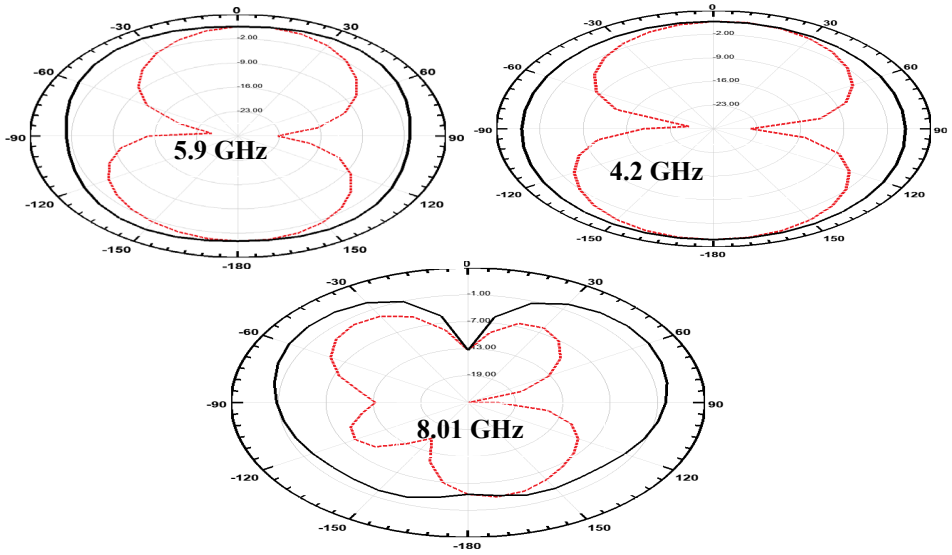

FIGURE 9. Simulated 2D radiation pattern E-Plane in dashed line at 5.84 GHz, 4.2 GHz, AND 8.01 GHz.

communication standards, including 5G sub-6 GHz bands (N79, N96, N102, N104, N46, N47), as well as WiMAX, WLAN, Wi-Fi 6, Wi-Fi 6E, DSRC for vehicular networks, and early 6G ranges.

The measured and simulated VSWR values are depicted in Fig. 8. It is observed that the proposed antenna exhibits recommended VSWR values (VSWR < 2) within the operating bandwidth for both simulated and measured results. Notably, minimal measured VSWR values are observed at 4.33 GHz (VSWR = 1.57), 5.97 GHz (VSWR = 1.22), and 8.04 GHz (VSWR = 1.5).

Fig. 9 shows the simulated two–dimensional radiation patterns of the antenna at 5.84 GHz, 4.2 GHz, and 8.01 GHz. The dashed curves represent the E–plane, while the solid curves correspond to the H–plane. At 5.9 GHz and 4.2 GHz, the patterns are close to omnidirectional, which is favorable for maintaining stable coverage. At 8.01 GHz, the radiation becomes more directional with additional lobes, mainly due to higher–order mode effects. This behavior indicates that the antenna preserves good omnidirectional radiation in the intended operating band. Such a radiation behavior ensures that the antenna can provide stable coverage in different directions, which is particularly important for vehicular communication scenarios where reliable connectivity must be maintained regardless of the orientation of the transmitting or receiving units.

Fig. 10 displays the simulated radiation efficiency and peak gain versus frequency. The gain ranges approximately from 2.63 dB to 5.15 dB within the operating bandwidth, while the efficiency varies between 94% and 81% across the same frequency range.

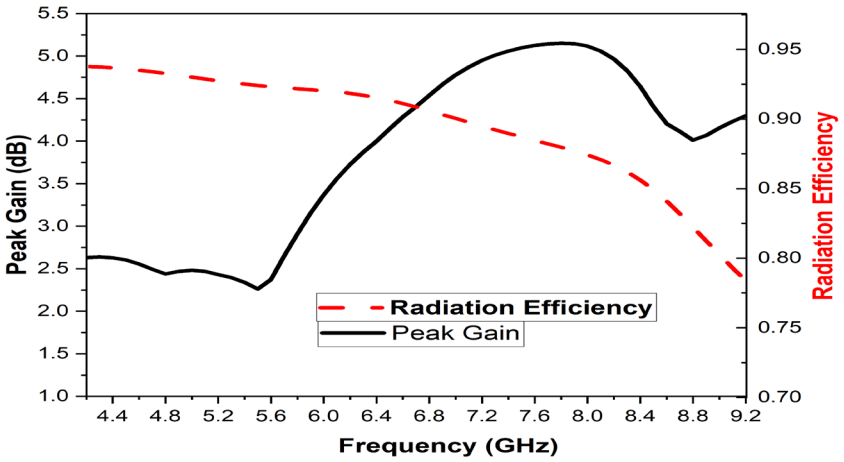

FIGURE 10. Simulated gain and radiation efficiency of the proposed antenna.

Table IV lists the frequency bands supported by the proposed antenna, covering several 5G sub-6 GHz allocations (N79, N96, N102, N104, N46, N47) as well as Wi-Fi 6E, Wi-Fi 7, DSRC/IEEE 802.11p, and early 6G ranges.

TABLE IV. Wireless applications of the proposed antenna

Name	Frequency range (GHz)
6G [24]	6.425–7.125
	7.125–8.4
N102 [25]	5.925–6.425
WIFI 6E [25]	5.925–7.125
N79 [4]	4.4–5
DSRC/IEEE802.11p [17]	5.85–5.95
N104 [4]	6.425–7.125
WIFI 7 [26]	5.17–5.835
	5.925–7.125
N96 [25]	5.925–7.425
N46 [25]	5.15–5.925
6G [25]	7.125–8.4
N47 [25]	5.855–5.925

Table V provides a comparative analysis between the proposed antenna and several previously reported designs in terms of physical dimensions, operational bandwidth, gain, substrate, and achieved bandwidth.

From the table, it can be observed that most earlier designs, such as those in [17],[27], represent a bandwidth often limited to values below 3.3 GHz. Although some studies, for example [28] and [29], achieved bandwidths around 2–3 GHz, they typically required larger structures or employed substrates like RT Droid or PET, which may increase fabrication costs. Similarly, designs in [30]–[31] show restricted bandwidths, with very low values in some cases (as small as 0.01 GHz), and in certain instances, gain values are either low or not explicitly reported.

By contrast, the proposed antenna presented in this work exhibits a wide operating bandwidth of 4.2-8.9 GHz, corresponding to a 4.51 GHz bandwidth, while maintaining compact dimensions of 36 × 36 mm² and using the cost-effective FR4 substrate. Furthermore, it achieves a stable gain ranging from 2.63 to 5.15 dB across the band.

TABLE V. Comparison the proposed antenna results with existing published studies

References	Physical dimensions	Gain	substrate	Bandwidth (GHz)
[32]	28.03 × 23.45	6.21	FR4	0.863
[28]	20 × 18	No mentioned	RT Droid	3.12
[29]	58 × 78	3	PET	2.01
[17]	31 × 28	3.2	FR4	3.3
[33]	55× 55	2	FR4	0.1 0.89
[27]	50 × 50	2.8–3.5 3.7–4.3	FR4	1.26 3.1
[30]	36 × 37	3.83, 0.537	FR-4	0.160, 0.220
[34]	40×40	6.05	FR4	0.1441
[31]	50×24	0.88, 2.6	Rogers RO400	0.01, 0.03
This work	36 ×36	2.63-5.15	FR4	4.7

The novelty of this work lies in the successful combination of broad impedance bandwidth, competitive gain, and compact size, realized through simple design modifications such as partial ground and slot incorporation. Unlike earlier antennas, which either compromise bandwidth or require more complex substrates, the proposed design balances performance, size, and fabrication cost, making it a strong candidate for modern multi-standard wireless communication systems including 5G, 6G, Wi-Fi 6/6E, DSRC, and WiMAX.

IV. Conclusion

A novel octagonal-shaped UWB patch antenna is presented in this article. The proposed antenna is analyzed, simulated, and measured. Based on the measured results, the proposed antenna operates from 4.2 GHz to 8.9 GHz. The suggested antenna covers vehicular communications. Additionally, the proposed antenna can cover other applications, including 5G sub-6GHz n79 band, IEEE 802.11ac/n WLAN, WiMAX band, Wi-Fi 6 based on the 802.11ax protocol, and WIFI 6E. The proposed design exhibits an omnidirectional radiation pattern; the obtained gain is about 2.6–3.15 dB.

Acknowledgements

This research received support from the Laboratory of Electrical Systems and Telecommunications, Faculty of Science and Technology, Cadi Ayyad University Marrakech (LSEEET-UCAM), working in collaboration with the Laboratory of Instrumentation Signals and Physical Systems (I2SP) within the Department of Physics, Faculty of Science at Cadi Ayyad University Marrakech, Morocco, and the Laboratory of Electrical Engineering at the Royal School of Aeronautics in Marrakesh, Morocco.

V. Reference

[1] P. K. Singh, S. K. Nandi, and S. Nandi, “A tutorial survey on vehicular communication state of the art, and future research directions,” *Vehicular Communications*, vol. 18, Aug. 2019, doi: 10.1016/j.vehcom.2019.100164.

[2] F. Ez-Zaki *et al.*, “Double Negative (DNG) Metamaterial-Based Koch Fractal MIMO Antenna Design for Sub-6-GHz V2X Communication,” *IEEE Access*, vol. 11, pp. 77620–77635, 2023, doi: 10.1109/ACCESS.2023.3296599.

[3] C. L. Mak, H. Wong, and K. M. Luk, “High-gain and wide-band single-layer patch antenna for wireless communications,” *IEEE Trans Veh Technol*, vol. 54, no. 1, pp. 33–40, Jan. 2005, doi: 10.1109/TVT.2004.838899.

[4] S. Lakrit, S. Das, A. El Alami, D. Barad, and S. Mohapatra, “A compact UWB monopole patch antenna with reconfigurable Band-notched characteristics for Wi-MAX and WLAN applications,” *AEU - International Journal of Electronics and Communications*, vol. 105, pp. 106–115, Jun. 2019, doi: 10.1016/j.aeue.2019.04.001.

[5] A. Ruengwaree, A. Ghose, and G. Kompa, “A novel UWB rugby-ball antenna for near-range microwave radar system,” *IEEE Trans Microw Theory Tech*, vol. 54, no. 6, pp. 2774–2778, Jun. 2006, doi: 10.1109/TMTT.2006.874892.

[6] A. E. C. Tan and M. Y. W. Chia, “Measuring human body impulse response using UWB radar,” *Electron Lett*, vol. 41, no. 21, pp. 1193–1194, Oct. 2005, doi: 10.1049/el:20052417.

[7] Z. Ma and Y. Jiang, “High-density 3d printable chipless rfid tag with structure of passive slot rings,” Jun. 01, 2019, *MDPI AG*. doi: 10.3390/s19112535.

[8] R. Xu, Y. Jin, and C. Nguyen, “Power-efficient switching-based CMOS UWB transmitters for UWB communications and radar systems,” *IEEE Trans Microw Theory Tech*, vol. 54, no. 8, pp. 3271–3277, Aug. 2006, doi: 10.1109/TMTT.2006.877830.

[9] C. Sharma and A. Sharma, “A Review Paper based on Various Bandwidth Enhancements Techniques for Ultra-Wide Band Antennas,” 2016. [Online]. Available: www.ijste.org

[10] S. M. Haque and H. Alam, “Further slot antenna miniaturization and bandwidth enhancement,” *International Journal of RF and Microwave Computer-Aided Engineering*, vol. 29, no. 7, Jul. 2019, doi: 10.1002/mmce.21732.

[11] R. Azadegan and K. Sarabandi, “A novel approach for miniaturization of slot antennas,” *IEEE Trans Antennas Propag*, vol. 51, no. 3, pp. 421–429, Mar. 2003, doi: 10.1109/TAP.2003.809853.

[12] Z. N. Low, J. H. Cheong, and C. L. Law, “Low-cost PCB antenna for UWB applications,” *IEEE Antennas Wirel Propag Lett*, vol. 4, no. 1, pp. 237–239, 2005, doi: 10.1109/LAWP.2005.852577.

[13] R. Azadegan and K. Sarabandi, “Bandwidth enhancement of miniaturized slot antennas using folded, complementary, and self-complementary realizations,” *IEEE Trans Antennas Propag*, vol. 55, no. 9, pp. 2435–2444, Sep. 2007, doi: 10.1109/TAP.2007.904086.

[14] M. Gopikrishna, D. D. Krishna, C. K. Aanandan, P. Mohanan, and K. Vasudevan, “Compact linear tapered slot antenna for UWB applications,” *Electron Lett*, vol. 44, no. 20, pp. 1174–1176, 2008, doi: 10.1049/el:20082269.

[15] S. Sadat, M. Fardis, F. Geran, G. Dadashzadeh, N. Hojjat, and M. Roshandel, “A Compact Microstrip Square-Ring Slot Antenna for UWB Applications.”

[16] Institute of Electrical and Electronics Engineers. Peru Section and Institute of Electrical and Electronics Engineers, *Proceedings of the 2017 IEEE XXIV International Congress on Electronics, Electrical Engineering and Computing (INTERCON) : Cusco, Peru, 15-18 August 2017*.

[17] F. Ez-Zaki, H. Belahrach, and A. Ghammaz, “Broadband microstrip antennas with Cantor set fractal slots for vehicular communications,” *Int J Microw Wirel Technol*, vol. 13, no. 3, pp. 295–308, Apr. 2021, doi: 10.1017/S1759078720000719.

[18] A. Pal and V. S. Tripathi, “Quad-element MIMO antenna with diverse radiation pattern characteristics and enhanced gain for 5.9 GHz V2X communications,” *AEU - International Journal of Electronics and Communications*, vol. 176, Mar. 2024, doi: 10.1016/j.aeue.2024.155119.

[19] K. Aliqab, A. Armghan, M. Alsharari, and M. H. Aly, “Highly decoupled and high gain conformal two-port MIMO antenna for V2X communications,” *Alexandria Engineering Journal*, vol. 74, pp. 599–610, Jul. 2023, doi: 10.1016/j.aej.2023.05.058.

[20] M. R. Jadhav and U. L. Bombale, “Design of F-Shaped Parasitic MIMO Antenna with DGS for Vehicle-to-Everything Communication,” *Progress*

in Electromagnetics Research B, vol. 109, pp. 41–56, 2024, doi: 10.2528/PIERB24070604.

[21] Y. B. Kim and H. L. Lee, "Compact planar phased array antenna for extended V2X communication coverage," *Alexandria Engineering Journal*, vol. 94, pp. 226–234, May 2024, doi: 10.1016/j.aej.2024.03.054.

[22] S. Rajpoot, G. S. Baghel, and M. V. Swati, "Design of a compact, wideband, Diagonal Square Fractal MIMO antenna for vehicular communication," *AEU - International Journal of Electronics and Communications*, vol. 202, Dec. 2025, doi: 10.1016/j.aeue.2025.156023.

[23] C. A. Balanis, *ANTENNA THEORY ANALYSIS AND DESIGN THIRD EDITION*. [Online]. Available: www.copyright.com.

[24] K. L. Wong, Y. H. Hsu, C. Y. Lee, and W. Y. Li, "Wideband 4-Port Patch Antenna Module Based Compact 8-Port Two-Module Antenna for 6G Upper Mid-Band 8 × 4 Device MIMO With Enhanced Spectral Efficiency," *IEEE Access*, vol. 12, pp. 88976–88991, 2024, doi: 10.1109/ACCESS.2024.3419549.

[25] H. Abbaoui, A. Ghammaz, H. Belahrach, and R.-J. El Bakouchi, "Design and simulation of a low return loss UWB CPW-fed patch antenna for mobile wireless communications," *ITM Web of Conferences*, vol. 52, p. 03007, 2023, doi: 10.1051/itmconf/20235203007.

[26] D. Lopez-Perez, A. Garcia-Rodriguez, L. Galati-Giordano, M. Kasslin, and K. Doppler, "IEEE 802.11be Extremely High Throughput: The Next Generation of Wi-Fi Technology beyond 802.11ax," *IEEE Communications Magazine*, vol. 57, no. 9, 2019, doi: 10.1109/MCOM.001.1900338.

[27] J. Ali *et al.*, "Cantor fractal-based printed slot antenna for dual-band wireless applications," *Int J Microw Wirel Technol*, vol. 8, no. 2, pp. 263–270, Mar. 2016, doi: 10.1017/S1759078714001469.

[28] T. Ali, M. Saadh Aw, and R. C. Biradar, "A Compact Bandwidth Enhanced Antenna Loaded with SRR For WLAN/WiMAX/Satellite Applications," 2018.

[29] A. Desai, "Flexible CPW fed transparent antenna for WLAN and sub-6 GHz 5G applications," no. August 2019, pp. 1–14, 2020, doi: 10.1002/mop.32287.

[30] S. K. Noor *et al.*, "A Patch Antenna with Enhanced Gain and Bandwidth for Sub-6 GHz and Sub-7 GHz 5G Wireless Applications," *Electronics (Switzerland)*, vol. 12, no. 12, Jun. 2023, doi: 10.3390/electronics12122555.

[31] I. Rosaline, P. Shastry, R. Venkatesan, and I. Tamilarasan, "Design and optimization of a miniaturized dual band rectenna for wireless power transfer applications," *Results in Engineering*, vol. 22, Jun. 2024, doi: 10.1016/j.rineng.2024.102199.

[32] T. Olawoye and P. Kumar, "A High Gain Antenna with DGS for Sub-6 GHz 5G Communications."

[33] Y.-Z. Hu, B.-J. Hu, and H.-L. Zhang, "A New Compact Dual-Band CP Antenna for GPS and DSRC Applications."

[34] S. Rana, N. Khurshid, S. K. Joy, S. I. Sourav, J. Hassan, and J. Nazmul, "A 3.5 GHz microstrip patch antenna design and analysis for wireless applications," *Indonesian Journal of Electrical Engineering and Computer Science*, vol. 32, no. 2, pp. 828–837, Nov. 2023, doi: 10.11591/ijeecs.v32.i2.pp828-837.